JOURNAL OF CATALYSIS **171,** 439–448 (1997)
ARTICLE NO. CA971829

Isotopic Oxygen Exchange between Dioxygen and MgO Catalysts for Oxidative Coupling of Methane

Takashi Karasuda and Ken-ichi Aika[1]

Department of Environmental Chemistry and Engineering, Interdisciplinary Graduate School of Science and Engineering, Tokyo Institute of Technology, 4259 Nagatsuta, Midori-ku, Yokohama 226, Japan

Received January 29, 1997; revised July 9, 1997; accepted July 14, 1997

The isotopic oxygen exchange between dioxygen and MgO based catalysts (Li/MgO, Zr/MgO, and MgO) was investigated at 773 to 1173 K in order to clarify the mechanism behind the generation of the active sites. The rate analysis was successful when two exchange steps having different rates (fast and slow) and different amounts of exchangeable (surface and lattice) oxygen atoms were assumed. The fast step was proposed as the exchange between dioxygen and the surface oxygen anion, whereas the oxide anion flow from the bulk to the surface was proposed for the slow step. However, both the MgO and Zr/MgO catalysts exhibited similar results regarding the two different rates and exchangeable oxygen atoms as well as their temperature dependencies. Zr/MgO had slightly higher rates due to the Zr^{4+} added, in contrast to the results for Li/MgO; a faster exchange per surface area and a larger amount of exchangeable oxygen (8.8 times as large as surface oxygen atoms at 1073 K). Li/MgO was proposed as having both O^-(MgO) and Li^+O^- as the active sites. The isotopic oxygen exchange (fast and slow) becomes measurable above ca 873 K, where hydrogen evolution starts during the TPD run (generation an O^- defect) while the oxidative coupling of methane (OCM) reaction becomes appreciable. This suggests that both the exchange and the OCM reactions occurred through the active sites of O^- produced at above 973 K. The exact rate of oxygen transfer in the exchange was much lower than the rate of the OCM reaction. From these results, we have concluded that the measurable "fast" exchange was the rate of exchange between the surface oxygen and the active center O^-, while the exchange between dioxygen and O^- (also a step of OCM) may be much faster.

INTRODUCTION

The synthesis of ethene from the partial oxidation of methane, i.e., the oxidative coupling of methane (OCM), is one of the most important processes in the chemical utilization of natural gas. Most of the active and selective catalysts for the OCM reaction are composed of two or three irreducible oxides, e.g., alkali metal oxides, alkali earth metal oxides, or rare earth metal oxides (1–4). Reducible oxides such as transition metal oxides are too active against methane which is easily oxidized further to CO_2. On the other hand, a part of the surface oxygen becomes active at high temperatures, reacting with methane even on irreducible oxides such as MgO. The special oxygen structure such as O^-, has been proposed as the active species.

It is known that O^-, which is an electron deficient oxygen ion, is formed from N_2O on the UV-irradiated (defect sites of) MgO (5–7). Although this O^- reacts with methane even at room temperature, the framework structure which retains the surface O^- itself is destroyed at temperatures higher than 523 K (8). Thus, it can be seen that the OCM reaction occurs on MgO only at high temperatures, usually 873–1073 K. If O^- is the active species, O^- or the surface structure accepting O^- must be generated only at high temperature on MgO catalytic systems.

An atomic randomization of dioxygen ($^{16}O_2 + {}^{18}O_2 = 2{}^{16}O{}^{18}O$) is known to occur at surprisingly low temperatures. The activity of ZnO becomes measurable when it is evacuated at 673 K after heat treatment in air at 1123 K. Although the rate of randomization is very rapid at 298 K (34×10^{12} molec. $cm^{-2}s^{-1}$), the activity decreases with the time of reaction (to 0.01×10^{12} molec. $cm^{-2}s^{-1}$) (9). If the reaction is carried out at 79 K, the activity remains constant at a high level (0.043×10^{12} molec. $cm^{-2}s^{-1}$), which corresponds to the stabilized activity at 698 K (0.06×10^{12} molec. $cm^{-2}s^{-1}$). Activation with high temperature treatment and deactivation on contact with oxygen suggests that the activity is due to a nonstoichiometric state of the oxide. Excess zinc seems to be responsible for the activity in this case. The reoxidation of excess zinc must be slow at 79 K, giving rise to a longer life in the activity. This is an example of which the active site structure is stable at low temperature, but it may be destroyed at medium temperatures and regenerated at high temperatures. Similar activation upon high-temperature evacuation can also be observed with MgO (10).

O^- (stable at high temperature) has been reported to be produced by doping with alkali metal ions (11) or by dissolving water as impurities (12) in the MgO lattice. The Li^+O^-

[1] To whom correspondence should be addressed. E-mail: kenaika@chemenv.titech.ac.jp.

0021-9517/97 $25.00

center in MgO has been observed by ESR and proposed as the active center of the OCM reaction (1, 11). Freund *et al.* have shown that high purity MgO contains excess amounts of oxygen (O^-) after decomposing impurity water evolving hydrogen (12, 13). P-type semiconductive oxides ($O^{2-} + h^+ = O^-$) have also been shown to be active and selective OCM catalysts (14). However, the production mechanism of the active (defect) site has yet to be studied in detail.

Here, we have focused our attention on MgO as a representative irreducible oxide for the OCM catalyst and have attempted to clarify the production mechanism of the active site. The authors have reported that the conductivity of MgO and Li/MgO are related to the defect structure produced by the decomposed impurity H_2O dissolved in the MgO lattice (15). The electric conduction is considered due to proton jumping at low temperatures, while hole conductivity prevails at high temperatures, where H_2O is dissolved in MgO (step 1 in Fig. 1) and the hole ($O^{2-} + h^+ = O^-$) is produced through H_2 evolution (step 2 in Fig. 1).

During the OCM reaction, O^- (or hole + O^{2-}) reacts with methane to produce methyl radical and OH^- (step 3 in Fig. 1). Two methyl radicals combine to form ethane (and then ethene). The produced OH^- is removed as H_2O leaving the defect (step 4 in Fig. 1) and dioxygen reproduces O^- again (step 5 in Fig. 1). If methane is not present but dioxygen is at the OCM temperature (step 5 in Fig. 1), then the reverse reaction (step 6 in Fig. 1) can be observed through the isotopic exchange. Thus, the isotopic exchange between dioxygen and MgO provides significant information on the active center of the OCM reaction.

Many authors have studied the isotopic oxygen exchange between MgO-based catalysts and dioxygen. Heinemann *et al.* (16) have reported on isotopic oxygen exchange over Li/MgO using TPIE (temperature programmed isotope exchange). Two types of active surface sites were found: a single exchange and a multiple exchange. Yanagisawa *et al.* (17) have also proposed O^- and O_2^{2-} as a single exchange and a multiple exchange over UV-irradiated MgO by TD (thermal desorption) studies, and Marcelin *et al.* (18) have studied MgO and Li/MgO using steady-state isotopic transient kinetic analysis (SSITKA).

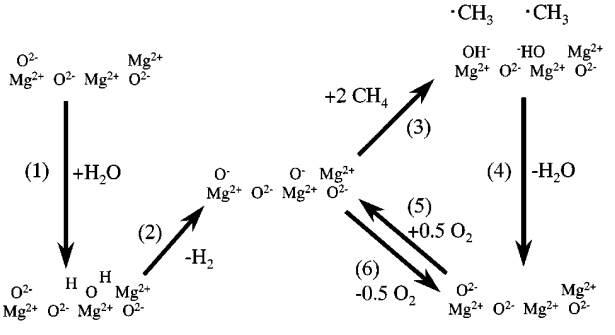

FIG. 1. Model of active center generation and the OCM reaction model.

In this paper, we have studied both temperature programmed desorption (TPD) and the isotopic oxygen exchange reaction over three MgO based catalysts; Li/MgO (*p*-type semiconductor, active and selective catalyst), Zr/MgO (*n*-type semiconductor), and MgO (reference sample). We have carried out comparative TPD, the isotopic exchange, and the OCM reaction studies, and we have discussed the nature of these three catalysts.

EXPERIMENTAL

Catalyst Preparation

Li (1 mol%)/MgO, Zr (1 mol%)/MgO, and MgO catalysts were prepared by an impregnation method from $LiNO_3$ (Kanto Chemicals, 99.96%), $ZrO(NO_3)_2 \cdot H_2O$ (Kanto Chemicals, 99.96%), and MgO (Soekawa Chemicals, 99.96%) (15). The catalysts were baked in air at 1273 K for 24 h and used for temperature programmed desorption (TPD) experiments and isotopic oxygen exchange. The BET surface area was measured by N_2 adsorption. The surface oxygen atom number ($N_{MgO(s)}$) was estimated as

$$N_{MgO(s)} = \frac{\text{Sur. area}}{\left(r_{Mg^{2+}} + r_{O^{2-}}\right)^2} \times 0.5, \qquad [1]$$

where the ionic radius are $r_{Mg^{2+}} = 0.72$ Å, $r_{O^{2-}} = 1.40$ Å.

OCM Reaction

The catalysts (0.2 g) were pretreated in a quartz reactor under a flow system at 1073 K for 1 h in He flow (20 ml min^{-1}). The OCM reactions were performed in the flow system with the reactant gas (CH_4/Air/He = 16/20/20 STPml min^{-1}) at various temperatures (673–1173 K). The reactant flow rates were controlled by mass-flow-controllers (UESHIMA · BROOKS Model 5896). The products were analyzed by on-line gas chromatographies (G. L. Science GC320 for TCD with packed WG-100 column and Shimadzu GC8A for FID with packed Porapak-Q column).

TPD

TPD was performed in a closed circulation system made of pyrex, which is similar to the system shown in Fig. 1 of past literature (19). The closed circulation system could be evacuated to pressures below 10^{-6} Torr by a rotary pump and a diffusion pump.

In order to eliminate water adsorbed on the surface, the catalysts (0.2 g) in a quartz reactor were evacuated at 1173 K for 1 h (first heating). Without further contact with H_2O, the TPD run was started from room temperature to 1173 K with a heating rate of 10 K min^{-1} (second heating). The desorption of H_2O, H_2, and O_2 which were due to the dissolved

water in the MgO based catalysts were analyzed by an on-line quadrupole mass spectrometer (NEVA NAG-515 mass filter). The amount of desorption during the second heating (TPD) depended on the conditions (temperature and time) of the first heating.

Isotopic Oxygen Exchange

The catalysts (0.2 g, 5.0 mmol of lattice oxygen) contained in a quartz reactor of the closed circulation system were evacuated at 1173 K for 1 h. After pretreatment, 8.2 Torr of the isotope oxygen molecule ($^{18}O_2$, 98.75%) was admitted to the upper part of the reactor (about 0.21 mmol of oxygen atom). The gas came into contact with the heated catalyst (673–1173 K) and was circulated through the catalyst bed in the closed circulation system by a magnetic circulation pump. A part of the gas (about 0.8%) was moved to the mass spectrometer through a sampling branch line. Sampling was done about 10 times; thus the total pressure subsequently decreased to 92% (we have ignored the change).

The isotope oxygen content (due to the exchange with the MgO catalysts) was measured up to 24 h by a quadrupole mass spectrometer (NEVA NAG-515 mass filter).

Analysis of Transfer Rate (R) and Exchangeable Amount of Oxygen Atoms

Independent from the mechanism, the oxygen atom exchange between the gas phase and the catalyst (Eq. [2]) can be analyzed (20) as

$$Mg^{16}O + {}^{18}O \text{ in dioxygen} = Mg^{18}O + {}^{16}O \text{ in dioxygen}. \quad [2]$$

The total mol number of the exchangeable oxygen atom of MgO (N_{MgO}) is composed by two isotope mol numbers, $n_{^{16}O}$ and $n_{Mg^{18}O}$ (Eq. [3]). Similar notations are also used for dioxygen, N_O, $n_{Mg^{16}O}$, and $n_{^{18}O}$ (Eq. [4]),

$$N_{MgO} = n_{Mg^{16}O} + n_{Mg^{18}O} \quad [3]$$

$$N_O = n_{^{16}O} + n_{^{18}O}, \quad [4]$$

where, N_{MgO}/N_O (defined as α) is constant under a reaction run (Eq. [5]),

$$\alpha = N_{MgO}/N_O. \quad [5]$$

The increase rate of ^{16}O in the gas phase (Eq. [6]) is proportional to R which is the total rate of oxygen transfer ($^{16}O + {}^{18}O$), and the ^{16}O-content difference between dioxygen ($F_{^{16}O} = n_{^{16}O}/N_O$) and MgO ($F_{Mg^{16}O} = n_{Mg^{16}O}/N_{MgO}$),

$$N_O \frac{dF_{^{16}O}}{dt} = R\left(F_{Mg^{16}O} - F_{^{16}O}\right). \quad [6]$$

The ^{16}O-content of MgO ($F_{Mg^{16}O}$) and that of dioxygen ($F_{^{16}O}$) should reach the same value at the equilibrium (*e*, equilibrium),

$$\left(F_{Mg^{16}O}\right)_e = (F_{^{16}O})_e = \frac{n_{Mg^{16}O} + n_{^{16}O}}{(1+\alpha)N_O} = \frac{n^{16}_{total}}{(1+\alpha)N_O}. \quad [7]$$

$F_{Mg^{16}O}$ at time t is also expressed as

$$F_{Mg^{16}O} = (F_{^{16}O})_e \frac{1+\alpha}{\alpha} - \frac{F_{^{16}O}}{\alpha}. \quad [8]$$

Equation [6] is transformed by substituting $F_{Mg^{16}O}$ with Eq. [8] as

$$N_O \frac{dF_{^{16}O}}{dt} = R\left(\frac{1+\alpha}{\alpha}\right)((F_{^{16}O})_e - F_{^{16}O}) \quad [9]$$

which can be integrated to give

$$\ln \frac{(F_{^{16}O})_e - (F_{^{16}O})}{(F_{^{16}O})_e - (F_{^{16}O})_0} = -R\left(\frac{1+\alpha}{\alpha}\right)\frac{t}{N_O}, \quad [10]$$

where $(F_{^{16}O})_0$, $(F_{^{16}O})$, and $(F_{^{16}O})_e$ are the ^{16}O-content of dioxygen at time 0, t, and infinite (24 h), respectively. When the left-hand side of Eq. [10] is plotted as a function of t, the slope is $-R(1+\alpha)\alpha^{-1}N_O^{-1}$.

RESULTS

OCM Reaction

The catalytic performances are shown in Figs. 1 to 4 and summarized in Table 1. Li/MgO has the highest and Zr/MgO has the lowest selectivity for C_2 production among the three catalysts, as has been reported. The C_2 yield on Li/MgO even reaches 34% under these conditions.

The temperature dependence of C_2 hydrocarbon production, CH_4 conversion, and O_2 conversion over MgO are shown in Fig. 2. CH_4 conversion, C_2 hydrocarbon selectivity, and O_2 conversion were increased extensively at above 973 K. CH_4 conversion was not increased when the reaction temperature was increased above 1073 K, where most of the dioxygen was consumed. On the other hand, the C_2 hydrocarbon selectivity decreased above 1073 K.

TABLE 1

Catalytic Activity over MgO-Based Catalysts[a] for the OCM Reaction[b] at 1073 K

	Conversion/%		Selectivity/%				
Catalyst	CH_4	O_2	C_2H_4	C_2H_6	CO	CO_2	C_2 yield/%
MgO	39.2	100.0	54.9	23.4	21.7	0.0	30.7
Li/MgO	39.6	87.1	61.8	24.7	3.6	9.9	34.3
Zr/MgO	35.2	94.5	45.9	20.4	8.6	25.2	23.3

[a] Pretreated under He of 20 cm^3min^{-1} and at 1073 K for 1 h.
[b] Feed gas: $CH_4/Air/He = 16/20/20$ cm^3min^{-1}.

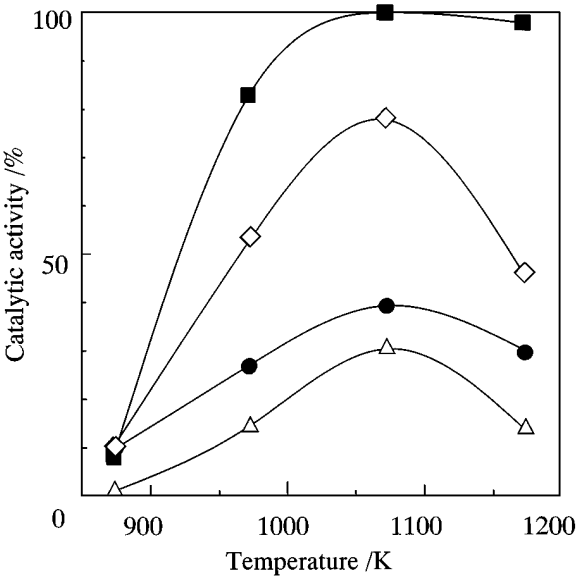

FIG. 2. Temperature dependence of MgO activity for OCM reaction; reactant gas (CH_4/Air/He = 16/20/20 cm^3min^{-1}), MgO = 0.2 g, CH_4 conversion (●), O_2 conversion (■), C_2 selectivity (◇), C_2 yield (△).

The temperature dependence of C_2 hydrocarbon production, CH_4 conversion, and O_2 conversion over Li/MgO are shown in Fig. 3. The CH_4 conversion and C_2 hydrocarbon selectivity began to increase at 973 K, similarly to MgO.

The temperature dependence of C_2 hydrocarbon production, CH_4 conversion, and O_2 conversion over Zr/MgO are shown in Fig. 4. Zr/MgO was even found to be active to produce C_2 hydrocarbon at such low temperatures as 873 K, probably because the O^{2-}, counterpart of Zr^{4+}, is more active than that of Mg^{2+}. The C_2 selectivity on Zr/MgO does not increase but that on Li/MgO and MgO increases above 973 K.

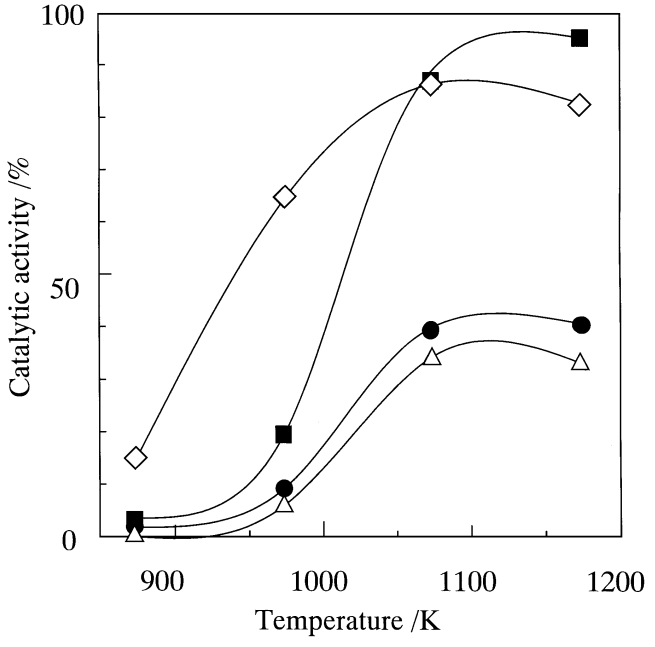

FIG. 3. Temperature dependence of Li/MgO activity for OCM reaction; reactant gas (CH_4/Air/He = 16/20/20 cm^3min^{-1}), MgO = 0.2 g, CH_4 conversion (●), O_2 conversion (■), C_2 selectivity (◇), C_2 yield (△).

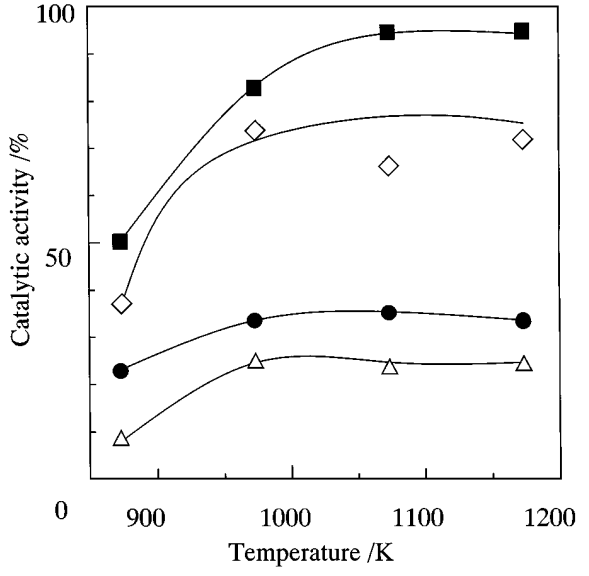

FIG. 4. Temperature dependence of Zr/MgO activity for OCM reaction; reactant gas (CH_4/Air/He = 16/20/20 cm^3min^{-1}), MgO = 0.2 g, CH_4 conversion (●), O_2 conversion (■), C_2 selectivity (◇), C_2 yield (△).

TPD

After the first heating (1173 K, 1 h), the sample was cooled down to the room temperature and the second heating (TPD) was carried out. The TPD spectra of H_2O and H_2 from the three catalysts are shown in Fig. 5. O_2 desorption could not be observed. The TPD products (H_2O and H_2) are molecules which were not eliminated by the first heating. As is seen from Fig. 5, H_2O could be desorbed at low temperatures from any MgO based catalysts, while H_2 (probably a decomposition product of H_2O) was desorbed only at high temperatures (above 973 K). H_2 starts to be desorbed at a temperature 200 degrees higher than the peak temperature of H_2O desorption, so that the H_2 observed by MS was not due to the fragmentation of H_2O. Among these catalysts the TPD profiles of H_2 were similar to each other (suggesting that H_2 comes from H_2O in MgO), while the H_2O TPD spectra were found to be distinctly different.

Isotopic Oxygen Exchange between Dioxygen and the MgO Catalysts

The time course of the isotope concentration of dioxygen was measured for the three catalysts at various temperatures (673–1173 K). The results for MgO at 973 K are shown in Fig. 6. The $^{18}O_2$ percentage decreases from 97 to

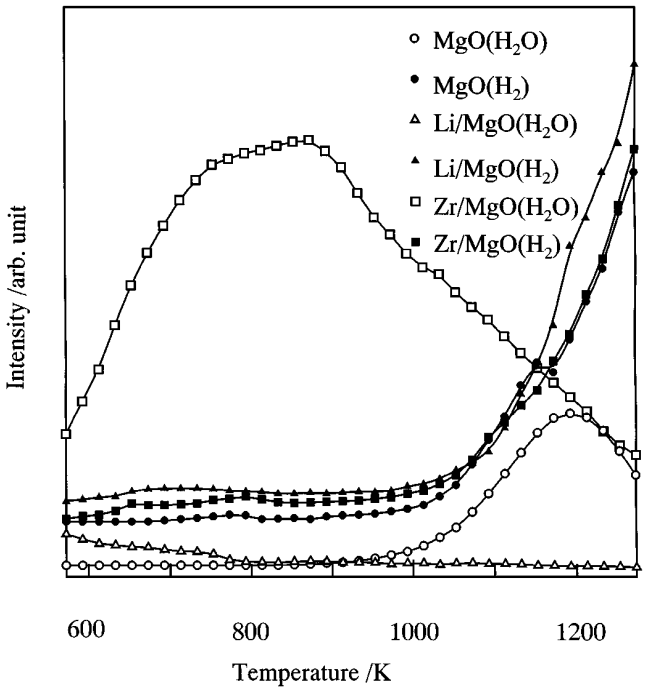

FIG. 5. TPD of H_2O (open symbol) and H_2 (closed symbol) from various MgO-based catalysts with a heating rate of 10 K min^{-1}.

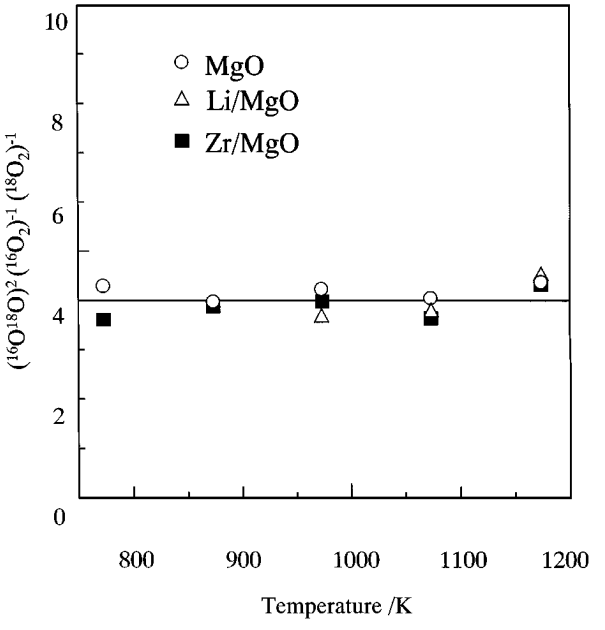

FIG. 7. Temperature dependence of the value of $(^{16}O^{18}O)^2(^{16}O_2)^{-1}$ $(^{18}O_2)^{-1}$ at 24 h on MgO-based catalysts.

29 in 480 min, while $^{16}O^{18}O$ and $^{16}O_2$ increase from 3 to 50% and from 0 to 21%, respectively, due to the exchange with the oxide oxygen (MgO). The value of $(^{16}O^{18}O)^2$ $(^{16}O_2)^{-1}(^{18}O_2)^{-1}$ is also plotted in Fig. 7. The values are almost constant (4.0) throughout the exchange, which means dioxygen is randomized (dissociated) throughout the exchange. The isotope atom concentration in the dioxygen was calculated from the result shown in Fig. 6, and the time course is shown in Fig. 8. We can see how the oxygen atom transfer occurs between dioxygen and MgO.

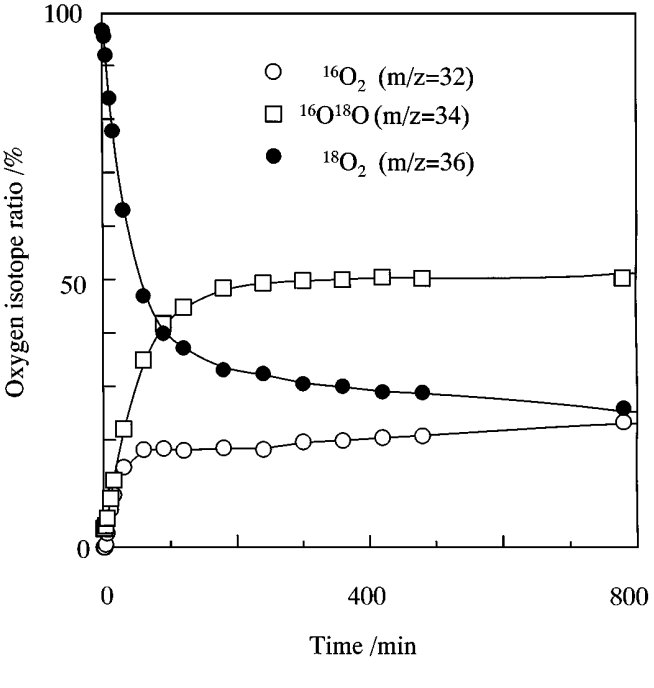

FIG. 6. Time course of oxygen isotope molecules ratio in gas phase over MgO at 973 K; $P_{O_2} = 8.2$ Torr, MgO = 0.2 g.

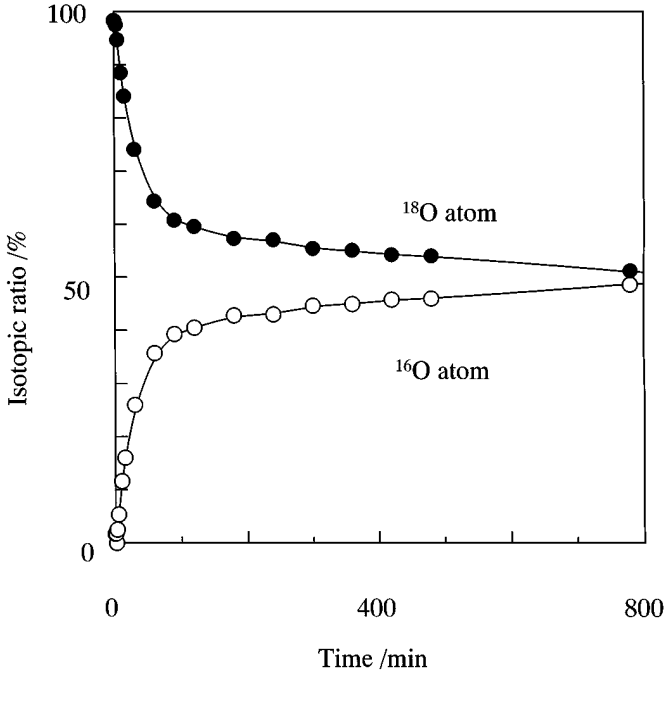

FIG. 8. Time course of isotope oxygen ratio in gas phase over MgO at 973 K; $P_{O_2} = 8.2$ Torr, MgO = 0.2 g.

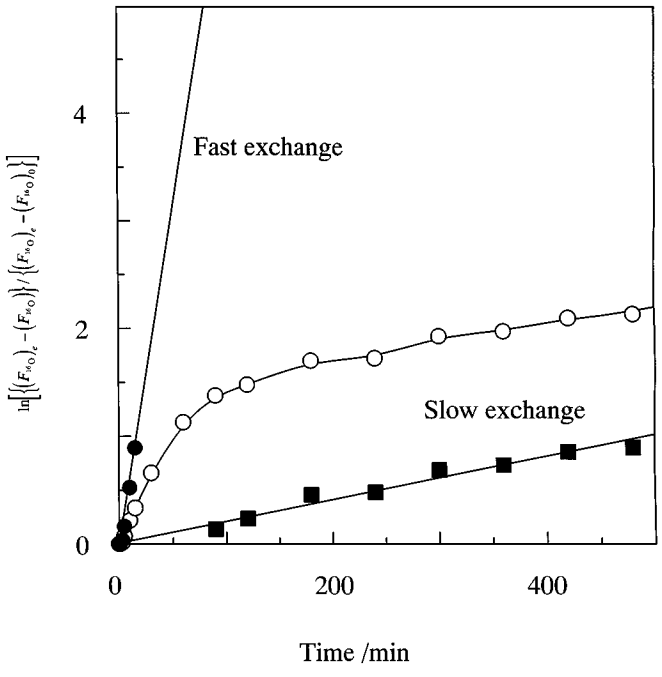

FIG. 9. Time course of $\ln[\{(F_{^{16}O})_e - (F_{^{16}O})\}/\{(F_{^{16}O})_e - (F_{^{16}O})_0\}]$; $(F_{^{16}O})_0$, $(F_{^{16}O})$, and $(F_{^{16}O})_e = {}^{16}O$ content in gaseous O_2 at time 0, t, and ∞, respectively, over MgO at 973 K; $P_{O_2} = 8.2$ Torr, MgO = 0.2 g.

In order to determine the rate of oxygen exchange, the left-hand side of Eq. [10] is calculated for each measurement and is shown in Fig. 9 (open symbol). Unexpectedly, the plot (open symbol) was not straight. The line can be seen to be folded with the slope declining. This suggests that the oxygen exchange is composed of at least two steps: a fast exchange of dioxygen with a small part of MgO and a slow exchange with a larger part of MgO. At the beginning the ^{16}O-content increases appreciably due to a fast exchange, but soon the process reaches an equilibrium and the slow process becomes observable.

The exchange model of the two stages in shown in Fig. 10, i.e., the fast exchange with an *a*-group O in MgO and the slow exchange with a *b*-group O in MgO. The amount of

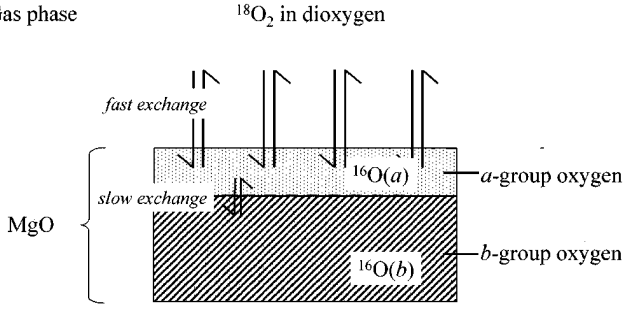

FIG. 10. The two-stage oxygen atom exchange model between dioxygen and MgO.

TABLE 2

Rate of Fast Isotopic Exchange (R_a) and Slow Exchange (R_b) between Dioxygen and MgO-Based Catalysts: The Unit is μmol min^{-1}g-cat^{-1}

Catalyst	Surface area/ $m^2\,g^{-1}$	Temperature/K	773	873	973	1073	1173
MgO	23.5	R_a:	0.96	2.14	5.00	6.17	7.64
		R_b:	0.11	0.14	0.19	0.20	0.39
Li/MgO	0.55	R_a:	—	—	0.16	0.36	1.10
		R_b:	—	0.01	0.06	0.17	0.38
Zr/MgO	19.7	R_a:	0.78	1.80	6.13	10.08	12.46
		R_b:	0.16	0.37	0.30	0.25	0.31

fast-exchangeable oxygen ($N_{MgO(a)}$) was tentatively estimated, assuming the equilibrium was reached at the time where the line clearly bends (80 min in the case of MgO at 973 K, Fig. 8). At this moment the ^{16}O-content in MgO(a) and that in dioxygen are the same $(F_{^{16}O(a)})_e$,

$$\left(F_{^{16}O(a)}\right)_e = \frac{n_{^{16}O} + n_{Mg^{16}O(a)}}{N_O + N_{MgO(a)}}. \qquad [11]$$

Substituting $(F_{^{16}O(a)})_e$ into $(F_{^{16}O})_e$ in Eq. [10], Eq. [12] is

$$\ln \frac{\left(F_{^{16}O(a)}\right)_e - (F_{^{16}O})}{\left(F_{^{16}O(a)}\right)_e - (F_{^{16}O})_0} = -R_a\left(\frac{1+\alpha_a}{\alpha_a}\right)\frac{t}{N_O}, \qquad [12]$$

$$\alpha_a = N_{MgO(a)}/N_O \qquad [13]$$

This relation was plotted as a black circle in Fig. 9, where a straight line was obtained. The slope gives R_a. The results are listed in Table 2. The amount of slow-exchangeable oxygen ($N_{MgO(b)}$) was also calculated, assuming the equilibrium was attained at 24 h. The slow exchange reaction becomes visible after 80 min. The ^{16}O content in the equilibrium for the slow exchange $(F_{^{16}O(b)})_e$ was determined as the value at the 24-h run.

$$\left(F_{^{16}O(b)}\right)_e = \frac{n_{^{16}O} + n_{Mg^{16}O(a)} + n_{Mg^{16}O(b)}}{N_O + N_{MgO(a)} + N_{MgO(b)}}. \qquad [14]$$

Substituting $(F_{^{16}O(b)})_e$ into $(F_{^{16}O})_e$ in Eq. [10], Eq. [15] is

$$\ln \frac{\left(F_{^{16}O(b)}\right)_e - (F_{^{16}O})}{\left(F_{^{16}O(b)}\right)_e - \left(F_{^{16}O(a)}\right)_e} = -R_b\left(\frac{1+\alpha_b}{\alpha_b}\right)\frac{t}{N_O}, \qquad [15]$$

$$\alpha_b = \frac{N_{MgO(b)}}{N_O + N_{MgO(a)}}; \qquad [16]$$

$\ln[\{(F_{^{16}O(b)})_e - (F_{^{16}O})\}/\{(F_{^{16}O(b)})_e - (F_{^{16}O(a)})_e\}]$ for t should form a straight line through point zero. This relation is plotted as a black square in Fig. 9. A straight line was obtained and the slope gives R_b, which is shown in Table 2. $N_{MgO(a)}$

TABLE 3

Relative Ratio of the Fast Exchangeable Oxygen Number against the Surface Oxygen ($N_{MgO(a)}/N_{MgO(s)}$) and That of Slow Exchangeable Oxygen Number (in 24 h) against the Total Lattice Oxygen ($N_{MgO(b)}/N_{MgO}$) as a Function of the Temperature

Catalyst	Surface area/ $m^2\ g^{-1}$	Oxygen number/ mmol g^{-1} O_s	Oxygen number/ mmol g^{-1} O_{bulk}	Temperature/K	773	873	973	1073	1173
MgO	23.5	0.435	—	$N_{MgO(a)}/N_{MgO(s)}$	0.2	1.0 (10)[a]	1.4	2.1	2.4
		—	4.96	$N_{MgO(b)}/N_{MgO}$	0.014	0.019	0.021	0.042	0.08
Li/MgO	0.55	0.010	—	$N_{MgO(a)}/N_{MgO(s)}$	— (8)[a]	— (10)[a]	3.7	8.8	35
		—	4.96	$N_{MgO(b)}/N_{MgO}$	—	0.0013	0.010	0.031	0.13
Zr/MgO	19.7	0.364	—	$N_{MgO(a)}/N_{MgO(s)}$	0.6	1.5	2.3	3.5	4.0
		—	4.96	$N_{MgO(b)}/N_{MgO}$	0.017	0.020	0.020	0.038	0.059

[a] Surface/subsurface exchangeable oxygen measured by steady-state isotopic transient kinetic analysis (SSITKA) (Ref. (18)).

and $N_{MgO(b)}$ (exchangeable oxygen atom number) are also listed in Table 3. Similar experiments and analysis were carried out on MgO at different temperatures (773, 873, 1073, and 1173 K).

The same runs were performed for the other two catalysts, and similar dynamic performances were obtained. Thus, the same method was applied for all of the catalysts. These rates have been displayed in Table 2 and the numbers of the exchangeable oxygen are shown in Table 3. It is very interesting that these results are consistent with Marcelin's results analyzed by another method (SSITKA), and parts of their data are also shown in the same Table 3.

DISCUSSIONS

Electron Deficient Oxygen Formation through H_2 Desorption and OCM Reaction

A dissolved H_2O in the MgO lattice is known to decompose to produce only H_2 above 973 K which should leave electron-deficient lattice oxygen atoms accompanied by a defect (13). Among electron deficient oxygen anions (O_2^-, O_2^{2-}, O^-, and O_3^-), the dissociated one (O^-) should prevail at the high temperature.

The following desorption mechanism can be postulated for the dissolved H_2O in the MgO lattice. MgO contains H_2O, a part of which enters into the MgO lattice and further becomes $Mg(OH)_2$ (Eq. [17]). The desorption of H_2O is considered to come from the lattice water (Eq. [18]) and hydroxyls (Eq. [19]). For doped MgO, some water may also come from the surface hydroxyls related to the dopant (as will be discussed later). The desorption of H_2 must come from $Mg(OH)_2$ (Eq. [20]). After H_2 is desorbed, two O^- which are the active sites of OCM, remain on the surface of the MgO catalysts:

$$MgO + H_2O = MgO(H_2O) = Mg(OH)_2 \quad [17]$$

$$MgO(H_2O) \rightarrow MgO + H_2O \quad [18]$$

$$Mg(OH)_2 \rightarrow MgO + H_2O \quad [19]$$

$$Mg(OH)_2 \rightarrow Mg^{2+} + O_2^{2-} + H_2 \rightarrow Mg^{2+} + 2O^- + H_2. \quad [20]$$

As can be seen in Figs. 2 to 4, the OCM reaction becomes observable above about 923 K, while H_2 production (O^- formation) occurs above about 973 K in the TPD runs (Fig. 5). The OCM reaction is conducted at a fixed temperature, but, the TPD run is a dynamic process in the temperature change, so that the latter process may occur at higher temperatures (most probably 50°). Thus, the two processes seem to start at the same temperature (under the same conditions), where the O^--defect is generated. TPD corresponds to steps 1 and 2 in Fig. 1, while the OCM reaction corresponds to steps 3, 4, and 5. The H_2 desorption profile also resembles the profile of DC conductivity of the MgO catalysts (21). The authors have found a hydrogen isotope effect of the activation energy of DC conduction at high temperature regions, where an O–H rupture is the key step in generating the hole ($O^{2-} + h^+ = O^-$).

It is rather interesting that the three samples (MgO, Li/MgO, and Zr/MgO) showed the same H_2-TPD profile, but that the C_2 yields were different. It is considered that H_2 comes only from the MgO lattice while that of the OCM reaction is influenced by the dopant, if any. Li^+ makes another active structure (Li^+O^- center) which improves C_2 production, while Zr^{4+} supplies more active oxygen which may convert CH_4 to CO_2. The desorption of H_2O from the three MgO-based catalysts were different from each other, depending on the surface chemical nature probably due to the use of different dopants. A large amount of H_2O is desorbed from Zr/MgO.

Isotopic Oxygen Exchange between Dioxygen and MgO Catalysts: The Fast Exchange

As has been analyzed above, oxygen exchange can be reasonably explained by assuming two processes, a fast exchange and a slow exchange. As is evident from Fig. 6 (for

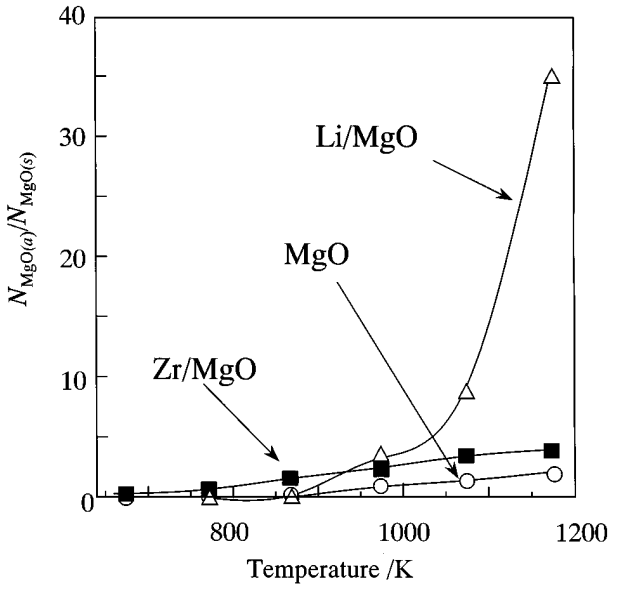

FIG. 11. Temperature dependence of active surface oxygen ($N_{MgO(a)}$) per surface oxygen ($N_{O(s)}$) calculated by the two-stage exchange model.

MgO at 973 K), the rate of oxygen exchange is fast during the first 80 min, and it is slower after that. The analyzed result of this case is shown in Fig. 9 (black points). From these analyses the following information could be obtained: the rate (R_a) and the amount ($N_{MgO(a)}$) for the fast exchange, and those for the slow exchange (R_b and $N_{MgO(b)}$). These four parameters were measured for other catalysts under various temperatures and summarized in Tables 2 and 3.

MgO and Zr/MgO seem to have similar numbers (R_a, R_b, $N_{MgO(a)}$, and $N_{MgO(b)}$). However, if we focus our attention on $N_{MgO(a)}$, the number of fast exchangeable oxygen atoms, those of Zr/MgO are much greater than those of MgO, especially at low temperatures (below 873 K). The amounts of exchangeable oxygen ($N_{MgO(a)}$) were divided by the surface oxygen numbers ($N_{MgO(s)}$) for these three catalysts ($N_{MgO(a)}/N_{MgO(s)}$), and are shown in comparison on Fig. 11 as a function of the temperature. The Zr^{4+} ions were found to have a decisive role in activating oxygen at low temperatures. Generally, the temperature dependence of the value (Fig. 11) resembles H_2-TPD (Fig. 5) and the OCM profile (Figs. 2–4). Thus, the oxygen becomes exchangeable and reactive with CH_4 when O^- is produced above 973 K. However, if Zr^{4+} is added to MgO (Zr/MgO), it becomes active even below 973 K, where O^{2-} of the counterpart of Zr^{4+} is considered to have some role in activating dioxygen (redox mechanism). It is interesting to note that $N_{MgO(a)}$ of MgO is identical to the surface/subsurface exchangeable oxygen of MgO at 873 K, carried out by another method (SSITKA) (18), as is shown in Table 2.

Li/MgO showed distinctly different results. The rate (R_a) and the number ($N_{MgO(a)}$) for Li/MgO seems to be much lower than those for MgO and Zr/MgO. However, if these are compared with the surface area bases, the rate and number for Li/MgO are rather higher than the others, as is shown in Fig. 11. Not only O^- (MgO) but also Li^+O^- plays a significant role in oxygen exchange. The amount of active surface oxygen species ($N_{MgO(a)}$) at 1073 K was 8.8 times as large as the amount of surface oxygen ($N_{MgO(s)}$) on Li/MgO. It is also interesting to point out that the surface/subsurface exchangeable O atoms studied by another method (SSITKA) also show high values, 10 at 873 K and 12 at 908 K for Li/MgO, corresponding to our fast-exchangeable oxygen (O(a)). The exact numbers are different but have a similar trend concerning the temperature and the kind of catalyst. The active surface oxygen seems to be composed of several layers near the surface.

Comparison of the Fast Exchange and the OCM Rate

The rates of the (fast) isotopic exchange are shown in Fig. 12. For comparison, the rates of OCM, which are calculated from O_2 conversion (although the O_2 conversion is high), are shown in Fig. 13. The experimental conditions of the isotopic exchange rate with the OCM reaction and the isotopic oxygen exchange were different in O_2 pressure (OCM reaction, 7 kPa; oxygen isotopic exchange, 1 kPa). The two reactions are also different thermodynamically; the former has a free energy cascade, while the latter is an entropy-expanding reaction just concerning isotopes. Considering such differences, the two rates can be compared as follows: (i) The observed OCM rate is about 780 and 40 times faster than the exchange rate for Li/MgO and MgO at 1073 K. (ii) If the rate is proportional to the O_2 concentration, the rate ratios must be reduced to about 110 and 6 for both catalysts. (iii) Since the OCM rate is measured

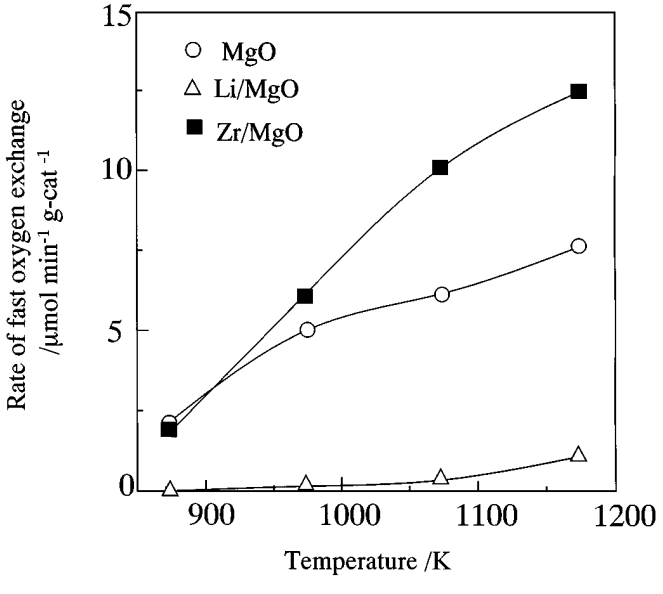

FIG. 12. Temperature dependence of the fast exchange rate (R_a) on MgO-based catalysts; $P_{O_2} = 8.2$ Torr, MgO = 0.2 g.

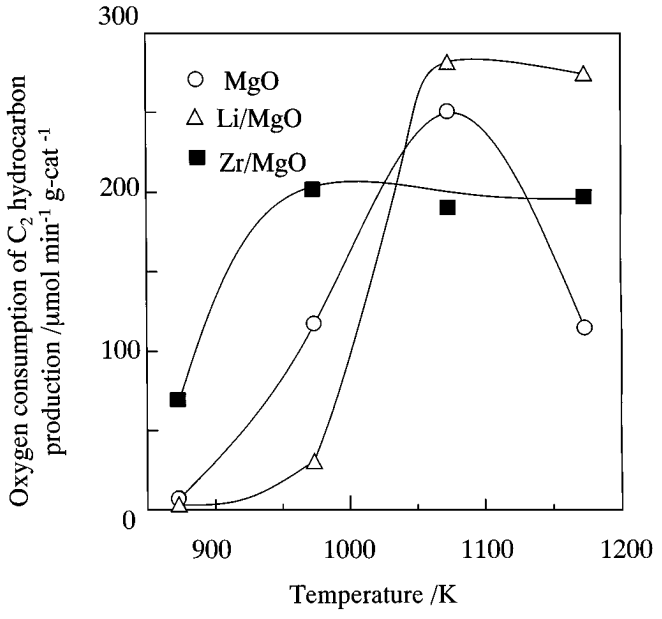

FIG. 13. Temperature dependence of oxygen consumption of C_2 hydrocarbon for the OCM reaction over MgO-based catalysts; reactant gas (CH_4/Air/He = 16/20/20 cm^3min^{-1}), MgO = 0.2 g.

at high conversion, the real (differential) rate at low conversion must be high (say 10 times), suggesting the oxygen transfers are higher in OCM than in the exchange (1000 and 60 times for Li/MgO and MgO).

As a result, the oxygen exchange rates (Fig. 12) were found to be much slower than the rate of OCM (Fig. 13). If the mechanism of Fig. 1 can be considered correct, OCM runs through steps 3, 4, and 5, evolving H_2O under dynamic conditions, while the exchange is either the rate of steps 5 and 6 under the adsorption–desorption equilibrium. The one-way rate under the equilibrium is usually slower than the rate of the dynamic reaction. However, the exchange rates seem to be much smaller than the reaction rates. Thus, the real rate of steps 5 and 6 were inconclusive because the amount of active species (probably O^-) are too small (especially for Li/MgO which has a very low surface area).

Proposal of the Very Fast Exchange

The "exchangeable oxygen" must contain, not only O^-, but also atoms surrounding O^-. The model is shown in Fig. 14. We can now classify the oxygen in MgO-based catalysts into three species: O^-; the oxygen atoms surrounding O^- (O(*a*)); and bulk oxygen (O(*b*)) by isotopic oxygen exchange. This classification seems to correspond to Marcelin's three classifications: the physical surface at which an exchange between the gas phase and the solid occurred; several subsurface atomic layers readily available for exchange; and the bulk oxide (18). We have proposed that their physical surface must be the actual active species (O^-).

Our measurements for fast exchange covers the following two processes, Eq. [21a] and Eq. [22a]:

$$O_2 \xrightarrow{\text{very fast}} O^- \quad \text{(reactive species)} \qquad [21a]$$

$$O^- \xrightarrow{\text{fast}} O(a) \quad \text{(lattice oxygen surrounding } O^-). \qquad [22a]$$

The work on DC conductivity (15, 21) also supports the above model. $^{16}O^-$ on the surface ($^{16}O(s)$) can be exchanged with dioxygen ($^{18}O_2$) through Eq. [21b]; the hole mobile mechanism supports the change of $^{18}O^-$ (i.e., $^{18}O^- = {}^{18}O^{2-} + h^{\bullet}$) to $^{16}O^{2-}$ at high temperatures as in Eq. [22b]:

$$^{18}O_2 + {}^{16}O^-_{(s)} \xrightarrow{\text{very fast}} {}^{16}O{}^{18}O + {}^{18}O^-_{(s)} \qquad [21b]$$

$$^{18}O^-_{(s)} + {}^{16}O^{2-}_{(s)} \xrightarrow{\text{fast}} {}^{18}O^{2-}_{(s)} + {}^{16}O^-_{(s)} \quad \text{(hole mobile)}. \qquad [22b]$$

If so, the real oxygen exchange between dioxygen and O^- may not be measured by this method, because of the small amount of surface O^-. One way to estimate the amount of O^- may be to determine the amount of H_2 evolved in a TPD run. However, this was unsuccessful due to the inaccuracy of mass analysis. Kazanski and co-workers have proposed an O_3^- intermediate for the "low temperature exchange" over V_2O_5/SiO_2 which is activated with hydrogen treatment followed by evacuation at 773 K (22):

$$^{16}O^- + {}^{18}O_2 \rightarrow {}^{16}O{}^{18}O{}^{18}O^- \rightarrow {}^{16}O{}^{18}O + {}^{18}O^-. \qquad [23]$$

The Slow Isotopic Oxygen Exchange

From the analysis of the two model steps of the isotopic oxygen exchange, the rate and amount of exchange were determined and are listed in Tables 2 and 3. Interestingly, for the three catalysts, the slow exchange rates were not strongly dependent on the temperature (Table 2). The rates of slow processes were about one-tenth those of the fast processes for any catalyst and conditions (Table 2). The amounts of exchangeable oxygen (for the slow process) reached 1 to 10% of the total MgO at high temperatures (Table 3). Thus, these oxygen ions must be the lattice anions, probably located near the defects, which increase at

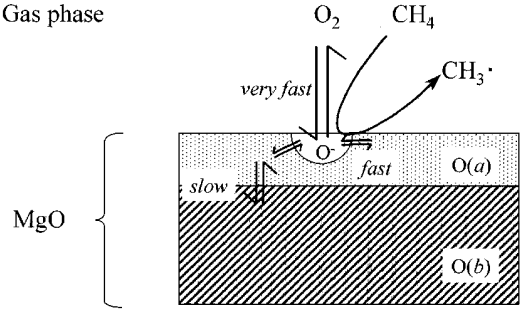

FIG. 14. Model of oxygen atom flux in MgO-based catalysts.

high temperature. These oxygen ions tend to be mobile at high temperatures (Eq. [24]). This process does not seem to relate with the OCM reaction:

$$^{18}O^{2-}_{(s)} + {}^{16}O^{2-}_{(bulk)} \xrightarrow{slow} {}^{16}O^{2-}_{(s)} + {}^{18}O^{2-}_{(bulk)} \quad \text{(mobil ions)}. \qquad [24]$$

CONCLUSION

We successfully analyzed the oxygen exchange reaction between dioxygen and MgO-based catalysts using a two-step mechanism. The exchange becomes active at the temperature where H_2 evolution starts at TPD (O^- formation). The OCM reaction also becomes active at a similar temperature.

Pure MgO is considered to become active when the impurity H_2O is decomposed to produce H_2 and O^- (defect). When Li is added, the additional active site Li^+O^- is produced in addition to O^-(MgO). Zr/MgO may produce additional active oxygen which also plays a role in converting CH_4 to CO_2.

The rate of oxygen transfer in the (fast) exchange was much lower than the rate of OCM reaction. We concluded that we were measuring the (fast) exchange rate between O^- and surface oxygen. The real rate of activation of dioxygen can be considered much faster. It was concluded that the OCM reaction occurs through such an activation step as is shown in Fig. 14.

ACKNOWLEDGMENTS

This work was supported in part by the International Research on Petroleum Refining and Technology sponsored by the Petroleum Industry Activation Center and the Ministry of Industry and Trade. The name of this foundation is the Petroleum Refinery and Highly Technical Use.

REFERENCES

1. Ito, T., and Lunsford, J. H., *Nature (London)* **314**, 721 (1985).
2. Iwamatsu, E., Moriyama, T., Takasaki, N., and Aika, K., *J. Catal.* **113**, 25 (1988).
3. Aika, K., Moriyama, T., Takasaki, N., and Iwamatsu, E., *J. Chem. Soc., Chem. Commun.*, 1210 (1986).
4. Otsuka, K., Jinno, K., and Moriwaka, A., *Chem. Lett.*, 499 (1985).
5. Aika, K., and Lunsford, J. H., *J. Phys. Chem.* **81**, 1393 (1977).
6. Wong, N. B., and Lunsford, J. H., *J. Chem. Phys.* **55**, 3007 (1971).
7. Williamson, W. B., Lunsford, J. H., and Naccache, C., *Chem. Phys. Lett.* **9**, 33 (1971).
8. Takita, Y., and Lunsford, J. H., *J. Phys. Chem.* **83**, 683 (1979).
9. Gorgoraki, V. I., Boreskov, G. K., Kasatkina, L. A., and Sokolovsky, V. D., *Kinet. Katal.* **5**, 120 (1964).
10. Boreskov, G. K., *Adv. Catal.* **15**, 286 (1964).
11. Ito, T., Wang, J.-X., Lin, C.-H., and Lunsford, J. H., *J. Am. Chem. Soc.* **107**, 5062 (1985).
12. Kathrein, H., and Freund, F., *J. Phys. Chem. Solids* **44**, 177 (1983).
13. Freund, F., and Wengeler, H., *J. Phys. Chem. Solids* **43**, 129 (1982).
14. Dubois, J.-L., and Cameron, J. C., *Appl. Catal.* **67**, 49 (1990).
15. Balint, I., and Aika, K., *J. Chem. Soc. Faraday Trans.* **91**, 1805 (1995).
16. Chang, Y.-F., Somorjai, G. A., and Heinemann, H., *J. Catal.* **142**, 697 (1993).
17. Yanagisawa, Y., Huzimura, R., Matsumura, K., and Yamabe, S., *Surf. Sci.* **242**, 513 (1991).
18. Peil, K. P., Goodwin, G., Jr., and Marcelin, G., *J. Catal.* **131**, 143 (1991).
19. Nishiyama, T., and Aika, K., *J. Catal.* **122**, 346 (1990).
20. Ozaki, A., "Isotopic Studies of Heterogeneous Catalysis." Kodansha, Tokyo, 1977.
21. Balint, I., and Aika, K., *in* "Natural Gas Conversion" (H. E. Cury-Hyde and R. F. Howe, Eds.), p. 177. Elsevier, Amsterdam, 1994.
22. Nikisha, V. V., Shelimov, B. N., Shvets, V. A., Griva, A. I., and Kazansky, V. B., *J. Catal.* **28**, 230 (1973).